IEEE Access
Multidisciplinary ⋮ Rapid Review ⋮ Open Access Journal

Received March 22, 2022, accepted April 6, 2022, date of publication April 12, 2022, date of current version April 20, 2022.

Digital Object Identifier 10.1109/ACCESS.2022.3166900

Characterizing the Steady-State Performance of AC Lines Through a Dimensionless Universal Model

PEDRO CRUZ-ROMERO, (Member, IEEE), ANTONIO GÓMEZ-EXPÓSITO, (Fellow, IEEE), AND JUAN CARLOS DEL-PINO-LÓPEZ

Departamento de Ingeniería Eléctrica, Universidad de Sevilla, 41004 Seville, Spain

Corresponding author: Pedro Cruz-Romero (plcruz@us.es)

This work was supported in part by the Research Grant PID 2020-116433RB-I00 (AEI) and Grant ENE2017-89669-R (AEI), and in part by CERVERA under Grant CER-20191019.

ABSTRACT This paper revisits the AC power line model. Based solely on three dimensionless parameters, a universal electrical model is first developed, which is valid for any kind of power line (overhead, underground/submarine or gas insulated), irrespective of its rated voltage and length. Then, by neglecting the shunt losses, compact expressions are obtained in terms of the two remaining parameters for all electrical magnitudes characterizing the steady-state behavior of any line, such as real and reactive power flows at both ends, losses, charging current, transmission capability, etc. As a result, universal parameterized curves are also provided, including the well-known PV and P-δ curves. Moreover, numerical ranges of defining parameters are obtained for a diversity of present or future line arrangements, rated voltages and lengths, which are then represented as clusters of points on the universal curves. Beyond educational purposes, the proposed formulation and the associated characteristic curves can be useful, at the planning or design stages, when a certain degree of parameter uncertainty is still present, in order to compare different designs, or when selecting the most suitable simplified model for a particular case study, before fully defining the line features (type of conductor, phase-to-phase clearance, type of configuration, insulation, etc.).

INDEX TERMS Charging current, distributed-parameter model, gas insulated line, steady-state stability limit.

LIST OF SYMBOLS

(LINE-SPECIFIC PARAMETERS AND MAGNITUDES)

b	Per-unit-length shunt capacitive susceptance (S/km).
B_s	Series susceptance (S). ($B_{s_{pu}}$: per-unit magnitude).
B_{sh}	Shunt susceptance (S). ($B_{sh_{pu}}$: per-unit magnitude).
$\cos\varphi$	power factor of the load connected to the receiving end.
C	Per-unit-length shunt capacitance (F/km).
g	Per-unit-length shunt conductance (S/km).
G_s	Series conductance (S). ($G_{s_{pu}}$: per-unit magnitude).
G_{sh}	Shunt conductance (S). ($G_{sh_{pu}}$: per-unit magnitude).
I_n	Maximum current (Thermally-limited or stability-limited) (A).
$\boldsymbol{I_r}$	RMS current phasor at the receiving end (A).
i_{sc}	Normalized sending-end charging current.
i_{smax}	Normalized sending-end current corresponding to $p_r = p_{rn}$.
$\boldsymbol{I_s}$	RMS current phasor at the sending end (A).
l	Length (km).
l_c	Critical length (km).
L	Per-unit-length series inductance (H/km).
p_l	Normalized active losses.
p_r	Normalized magnitude of $P_{r_{pu}}$.
$P_{r_{pu}}$	Per-unit receiving-end active power (pu).
p_{r0}	Normalized power at the receiving end when $q_l = 0$.
p_{rmax}	Value of p_r for $\delta = \delta_{max}$.
p_{rn}	Normalized magnitude of P_{rn}.

The associate editor coordinating the review of this manuscript and approving it for publication was Fabio Mottola.

P_{rn}	Maximum active power (thermally-limited or stability-limited) at the receiving end (MW).
p_s	Normalized magnitude of $P_{s_{pu}}$.
p_{sc}	Value of p_s for $p_r = q_r = 0$.
$P_{s_{pu}}$	Per-unit sending-end active power (pu).
q_l	Normalized reactive balance.
q_r	Normalized magnitude of $Q_{r_{pu}}$.
q_{sc}	Value of q_s for $p_r = q_r = 0$.
$Q_{r_{pu}}$	Per-unit receiving-end reactive power (pu).
Q_{rn}	Reactive power at the receiving end when active power is P_{rn} and $V_r = 0.95V_s$ (MW).
q_s	Normalized magnitude of $Q_{s_{pu}}$.
$Q_{s_{pu}}$	Per-unit sending-end reactive power (pu).
r	Per-unit-length series resistance (Ω/km).
R_s	Series resistance (Ω).
s_{sc}	Value of sending-end apparent power for $p_r = q_r = 0$.
SIL	Surge impedance loading.
x	Per-unit-length series inductive reactance (Ω/km).
V_r	RMS voltage at the receiving end of the line. ($V_{r_{pu}}$: per-unit magnitude).
V_s	RMS voltage at the sending end of the line. ($V_{s_{pu}}$: per-unit magnitude).
v_r	Normalized voltage at the receiving end of the line.
v_{rc}	Value of v_r for $p_r = q_r = 0$.
X_s	Series reactance (Ω).
y	Per-unit-length complex shunt admittance (S/km).
Y_s	Series admittance (S).
z	Per-unit-length complex series impedance (Ω/km).
Z_0	Characteristic impedance (Ω)Complex series impedance (Ω).
α	Attenuation constant (1/km).
β	Phase constant (1/km).
δ	phase difference between sending and receiving voltages (rad).
δ_{max}	steady-state stability limit angle (rad).
γ	Propagation constant (1/km).
κ_s	Coefficient of series losses (also named κ).
κ_{sh}	Coefficient of shunt losses.
τ	Coefficient of reactive balance.
ω	Angular frequency of electrical magnitudes (rad/s)

I. INTRODUCTION

Starting from the single-phase representation of two-port networks (customarily represented by the *ABCD* matrix), different distributed-parameter models of three-phase symmetrical lines have found widespread use, such as the π-equivalent, Γ-equivalent or T-equivalent circuits [1]. For a given frequency ($\omega = 2\pi f$), the steady-state behavior of a power line can be represented through an equivalent circuit which depends ultimately on four electrical parameters, namely the series resistance and reactance (r and $x = \omega L$), and the shunt conductance and susceptance (g and $b = \omega C$), all per unit length, along with the line length l (which is worth retaining as an additional parameter to duly analyze its role). Parametric studies that aim to be as universal as possible should, therefore, analyze the impact of these 4+1 parameters on the electrical performance of any line.

Historically, the presence of hyperbolic functions in the expressions of the *ABCD* matrix, and the lack of digital computers, led to the use of approximate expressions, obtained by retaining the first two or three terms of their series expansion. Alternatively, a long line can be divided into a finite number of short segments, each characterized by a lumped-parameter model, in which all parameters are proportional to the respective segment length. But none of those approximations can get rid of the five required parameters.

Simplified models, which take advantage of the large differences in parameter values found in several particular cases of practical interest, are routinely used, such as the four-parameter model (shunt conductance neglected), which is acceptable for virtually any overhead line, the three-parameter model (shunt admittance neglected), for relatively short overhead lines, or the lossless model (series resistance and shunt conductance neglected), usually adopted for long overhead lines rated at ultra high voltages [1].

Those approximations have proven useful in explaining a variety of power line behaviors, preferably in a graphical form to more easily capture the impact of each parameter. Additional parameterizations are frequently found, by considering for instance the rated voltage or external parameters, such as the power factor (or reactive power) of the load served by the line.

This paper develops an accurate positive-sequence analytical model, valid for any kind of AC line, which is based only on three dimensionless parameters. Such universal model leads to a rather simple algebraic formulation, from which the customary parameterized graphical analysis can be easily derived. Then, the performance of a generic line (voltage profile, transmission capability, reactive power internal balance, power losses, etc.), is fully characterized with the help of the proposed model.

The paper is divided as follows: Section II briefly provides the background (the classical distributed-parameter π-circuit). Section III reviews previous parametric studies that have used this formulation in its different simplifying variants. Section IV presents the new parameters and the corresponding dimensionless formulation of the line power flows. Section V presents the main analytical and graphical results derived from the application of the model on all types of lines, assuming the shunt conductance to be negligible. Finally, Section VI presents the conclusions.

II. DISTRIBUTED-PARAMETER π-CIRCUIT

The single-phase equivalent π-circuit of a power line, obtained from the *ABCD* matrix [1], is depicted in Fig. 1, where the total series impedance (Z_s) and half shunt admittance (Y_{sh}) can be expressed as nonlinear functions of five parameters, including the four per-unit-length values

(r, x, g and b) and the line length, l, as follows:

$$Z_s = R_s + jX_s = zl\frac{\sinh \gamma l}{\gamma l} = Z_0 \sinh \gamma l \tag{1}$$

$$Y_{sh} = G_{sh} + jB_{sh} = \frac{yl}{2}\frac{\tanh \frac{\gamma l}{2}}{\frac{\gamma l}{2}} = \frac{1}{Z_0}\tanh \frac{\gamma l}{2} \tag{2}$$

where $z = r + jx$, $y = g + jb$ and $\gamma = \sqrt{zy} = \alpha + j\beta$, $Z_0 = \sqrt{z/y}$ are known, respectively, as the propagation constant and the characteristic impedance. In the lossless case ($r = g = 0$), γ is purely imaginary ($\alpha = 0$) and Z_0 reduces to a resistance (R_0). When the line is loaded with a pure resistance equal to R_0, the operating point is known as Surge Impedance Loading (SIL), which is frequently used as a reference. It can be shown that any lossless line serving the SIL is perfectly balanced in terms of reactive power, and features a flat voltage profile [1].

For the purposes of this paper, the series admittance rather than the series impedance will be used:

$$Y_s = 1/Z_s = G_s - jB_s \tag{3}$$

Note the minus sign preceding B_s, intentionally used so that all line parameters are positive (this change of sign is not needed in (2) because $B_{sh} > 0$).

Accordingly, the current-voltage relationships for the single-phase circuit of Fig. 1 are as follows, when voltages are represented in polar coordinates:

$$\boldsymbol{I_s} = -(G_s - jB_s)V_r + [(G_s + G_{sh}) - j(B_s - B_{sh})]\, V_s\angle\delta$$
$$\boldsymbol{I_r} = (G_s - jB_s)V_s\angle\delta - [(G_s + G_{sh}) - j(B_s - B_{sh})]\, V_r$$

Then, the real and reactive power flows can be readily obtained from their definition ($P + jQ = \boldsymbol{VI}^*$). At this point, it is customary to adopt the per unit system, which has two main advantages: 1) all transformer ratios become 1:1 (i.e., all impedances/admittances are referred to a common framework); 2) single-phase and three-phase magnitudes are indistinguishable for balanced systems. When doing so, the power flows at the sending (input power) and receiving (output power) ends, in per-unit magnitudes, are given by:

$$P_{s_{pu}} = V_{r_{pu}}V_{s_{pu}}(B_{s_{pu}}\sin\delta - G_{s_{pu}}\cos\delta) + V_{s_{pu}}^2(G_{s_{pu}} + G_{sh_{pu}}) \tag{4}$$

$$Q_{s_{pu}} = -V_{r_{pu}}V_{s_{pu}}(B_{s_{pu}}\cos\delta + G_{s_{pu}}\sin\delta) + V_{s_{pu}}^2(B_{s_{pu}} - B_{sh_{pu}}) \tag{5}$$

$$P_{r_{pu}} = V_{r_{pu}}V_{s_{pu}}(B_{s_{pu}}\sin\delta + G_{s_{pu}}\cos\delta) - V_{r_{pu}}^2(G_{s_{pu}} + G_{sh_{pu}}) \tag{6}$$

$$Q_{r_{pu}} = V_{r_{pu}}V_{s_{pu}}(B_{s_{pu}}\cos\delta - G_{s_{pu}}\sin\delta) - V_{r_{pu}}^2(B_{s_{pu}} - B_{sh_{pu}}) \tag{7}$$

In addition to the four line parameters, each equation embeds four electrical variables (power, voltage magnitudes and phase difference) which, independently or combined, are to be considered in the parameterized curves.

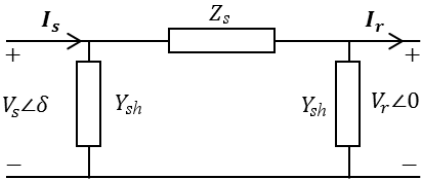

FIGURE 1. Equivalent π-circuit of a power line.

III. BRIEF REVIEW OF PARAMETRIC STUDIES

Since the beginnings of power engineering, the parametric analysis of lines has helped to better understand their electrical performance. Without claiming to be exhaustive, we summarize here some of those studies, focusing especially on aspects like parameters involved, simplifying assumptions and analytical and graphical results.

In [2] the aim of the parametric analysis was the estimation of the loadability characteristic curve (steady-state load capability versus length) of HV overhead lines (34.5−330 kV), obtaining empirically derived curves that are based on a predefined steady-state stability margin. In [3], a more analytical approach is performed, obtaining similar curves under the assumptions of lossless line and constant γ value for all line designs. This way, the load capability (in per-unit of SIL) is not dependent on per-unit-length parameters, being only a function of the line length and terminal voltages. Assuming a constant load power factor, it is possible to obtain simple curves of line loadability versus length, within voltage drop and stability limits. Moreover, the analysis of [2] is extended in [3] to EHV/UHV transmission lines, highlighting the fact that the simplifying assumptions are even more justified at those voltage levels. If the analysis is aimed at assessing the effect of the line design (single/double circuit, three/four-conductor bundle, etc.) on its loadability characteristic, then a curve for each design should be considered [4]. Recently, a general formulation of the loadability characteristic regions (thermal limit, voltage drop limit and stability limit) has been proposed [5].

Regarding high voltage cables (66-220 kV), simple and approximate analytical expressions for the critical length (l_c) are derived in [6] by neglecting the series impedance Z_s. Graphical representations of I_r/I_n versus l/l_c, where I_n is the cable ampacity, are plotted for a particular 220 kV, 2000 MCM high pressure, oil-filled pipe-type cable. Application of the same curves to other cross sections yields an acceptable error at voltages equal to or higher than 132 kV. When dry-type cables with low dielectric losses are rather considered, G_{sh} can be neglected for $l < 150$ km. In [7], the loadability and losses of compensated, three-core submarine cables with voltages between 132 and 400 kV are depicted versus the cable length, for a particular cross section of 1000 mm^2. In [8], an in-depth analysis of the behavior of umbilical cables with rated voltages between 35 and 150 kV and cable cross sections between 95 and 400 mm^2 is performed. The receiving end voltage and power, as well as the sending end current, are depicted versus the cable length in

order to highlight the limitation of power transfer due to the charging current.

We can conclude that the previous parametric studies have usually been devoted to analyzing a particular aspect of a certain type of line (e.g. long overhead line, high voltage underground cable, etc.), generally applying some modeling assumptions and representing relevant magnitudes (e.g., receiving active power or sending charging current versus length) for a particular voltage range and configuration. This work is not intended to enhance those specific studies (well established in the literature), but rather to develop a comprehensive analytical and graphical framework, based on the distributed parameter model, which is accurate enough for all types of lines. The proposed unified framework uses three dimensionless parameters, which can be reduced for practical purposes to two parameters only. As the values of those parameters lie in a predefined interval for each major category of line, it is possible to assess the performance of a certain line, real or hypothetical, even if its parameters are not precisely known, by resorting to typical or expected values.

IV. DIMENSIONLESS PARAMETERS AND POWER FLOWS

To begin with, the following reference power, known as the Static Stability Limit (SSL), or static transmission capacity, is introduced:

$$\mathrm{SSL} = V_{s_{pu}}^2 B_{s_{pu}}. \tag{8}$$

Note that, as the sending voltage is normally very close to the rated voltage, the SSL is mainly determined by the series admittance (i.e., by the tower/conductor configuration and line length). The reader should be aware that, by neglecting the series resistance (only valid for UHV lines), the SSL is also defined in some classical textbooks as $V_{s_{pu}}^2/X_{s_{pu}}$. While the reasons for the name of this reference power will be apparent later on, it is worth noting at this point that the SSL is generally much larger than the SIL, also used as an alternative reference power in the literature.

Then, the power flow relationships (4)-(7) are normalized by dividing both members of the equations by the SSL, leading to:

$$p_s = v_r(\sin\delta - \kappa_s\cos\delta) + (\kappa_s + \kappa_s\kappa_{sh}) \tag{9}$$
$$q_s = -v_r(\cos\delta + \kappa_s\sin\delta) + (1-\tau) \tag{10}$$
$$p_r = v_r(\sin\delta + \kappa_s\cos\delta) - v_r^2(\kappa_s + \kappa_s\kappa_{sh}) \tag{11}$$
$$q_r = v_r(\cos\delta - \kappa_s\sin\delta) - v_r^2(1-\tau) \tag{12}$$

where $v_r = V_{r_{pu}}/V_{s_{pu}}$ denotes the receiving voltage normalized with the sending voltage. The above normalized power flows constitute the basis of the universal model developed in this work. They are nonlinear functions of the normalized receiving voltage (v_r) and the phase angle difference between the two end buses (δ), along with three dimensionless parameters that will be introduced in the sequel.

A. COEFFICIENT OF SERIES LOSSES

This represents the relative size of the series conductance (resistance) with respect to the series susceptance (reactance):

$$\kappa_s = \frac{G_s}{B_s} = \frac{R_s}{X_s}\,. \tag{13}$$

The value of κ_s ranges, for any kind of realistic AC line, between 0.05 (UHV transmission level) and 1.5 (LV feeder).

B. COEFFICIENT OF SHUNT LOSSES

This is the ratio between the shunt and series conductance:

$$\kappa_{sh} = \frac{G_{sh}}{G_s}\,. \tag{14}$$

The value of κ_{sh} is generally negligible, except for UHV lines facing very special environmental conditions. If neglected, as is customarily done, then the active power line losses (p_l) are proportional to κ_s:

$$p_l = p_s - p_r = \kappa_s(1 + v_r^2 - 2v_r\cos\delta)\,. \tag{15}$$

C. COEFFICIENT OF REACTIVE POWER BALANCE

This ratio represents the relative size of the shunt susceptance with respect to the series susceptance:

$$\tau = \frac{B_{sh}}{B_s}\,. \tag{16}$$

A discussion follows, to better understand its range of values and role in the reactive power balance.

From (16), taking into account (1) and (2), a very accurate approximation (less than 0.3 % error for any kind of power line), can be derived as follows:

$$\tau \approx \frac{1}{4}bxl^2\frac{\sin\beta l}{\beta l}\left(3 - \frac{\sin\beta l}{\beta l}\right)(1+\kappa_s^2)\,. \tag{17}$$

The ratio $\sin\beta l/\beta l$ is always close to 1, whereas κ_s ranges between 0.05 and 1.5. Therefore, from (17), the following limits apply in practice:

$$0.5 \le \frac{\tau}{bxl^2} \le 1.6\,. \tag{18}$$

By giving extreme values to b, x and l we obtain the range of possible values for τ:

$$10^{-6} \le \tau \le 0.25\,, \tag{19}$$

Note that the (quadratic) effect of the line length on the electrical behavior of the line is integrated in this parameter, which explains its unusually wide range of variation if it has to cover all power lines of practical interest.

From (10) and (12) the reactive power balance of the line is given by

$$q_l = q_s - q_r = (1+v_r^2)(1-\tau) - 2v_r\cos\delta\,. \tag{20}$$

where a positive (negative) value means that the line has a deficit (surplus) of reactive power. Equation (20) compactly shows the important role of τ (and hence the line length) in the reactive power balance of the line, which justifies its name.

V. APPLICATIONS OF THE UNIVERSAL LINE MODEL

In this section, the steady-state electrical behavior of any kind of line, including the line loadability, efficiency, reactive power requirements, charging current, Ferranti effect and PV/QV/PQ curves, will be fully characterized based on the coefficients κ_s and τ. For this purpose, it will be assumed that $\kappa_{sh} = 0$ (i.e., $G_{sh} \ll G_s$). Hence, for simplicity of notation, κ_s will be named just κ in the sequel.

A total of 20 power lines (see Table 1), covering the three major types (overhead, underground/submarine and gas insulated), as well as a wide range of rated voltages (from 400 V to 1200 kV), have been considered to illustrate the analysis and annotate the resulting curves. For each line, the length l is selected from the top range of typical present or future values. Along with the parameters, Table 1 includes the values of the active power at the receiving end, P_{rn} (stability-limited in cases O6, O7 and O8, thermally-limited for the rest), as well as the reactive power Q_{rn} calculated so that $V_r = 0.95V_s$ for the given active power flow. Note that the reactive power is negative for overhead lines (i.e., it is also injected, rather than drawn, at the receiving end) and positive for cables, reflecting deficit and surplus, respectively. For the stability-limited lines, it is assumed that the maximum allowed phase angle difference is $\delta_{max}/2$, where δ_{max} denotes the value of δ corresponding to the theoretical steady-state transmission capacity, as discussed below.

The values of κ and τ, corresponding to the lines of Table 1, are shown in Table 2, where a general trend for the evolution of those parameters with type of line and voltage can be observed. For the three line types, the behavior of κ is similar, namely decreasing from higher voltages. This is explained from (13) and (1):

$$\kappa = \frac{R_s}{X_s} = \frac{\mathrm{Re}[zl\frac{\sinh\gamma l}{\gamma l}]}{\mathrm{Im}[zl\frac{\sinh\gamma l}{\gamma l}]} \approx \frac{\mathrm{Re}[zl]}{\mathrm{Im}[zl]} = \frac{r}{x}. \tag{21}$$

Typically, the ratio r/x decreases for increasing voltages, regardless the type of line. Note that, despite this general trend, there are particular cases, such as U3, departing from this rule of thumb, owing to the influence of other factors, like different conductor clearances in the underground case.

Regarding the evolution of τ with voltage and type of line, it is worth recalling from (18) that τ is basically proportional to bxl^2. For each type of line, the dependence with the square of length is the main reason behind the behavior of τ. For overhead lines, the increasing length with voltage of the cases of Table 1 explains the evolution of τ from O1 to O8. On the other hand, for the underground cables, the evolution of length against voltage is basically decreasing, so the behavior of τ is the same. Eventually, for GILs of Table 1 the length is again increasing with voltage, so τ will behave similarly.

For the same reason, when comparing lines of similar length, even of different voltages, the difference in τ will be due basically to the product bx. A good example is O4 and G4, both with the same length (150 km). From Table 2, the values of τ for O4 and G4 are 134 and 125, respectively, which are roughly in the same proportion as their product bx.

TABLE 1. Parameters of typical power lines (50 Hz, $g = 0$).

Name (1)	Volt. (kV)	l (km)	P_{rn} (MW)	Q_{rn} (Mvar)	r (mΩ/km)	x (mΩ/km)	b (μS/km)	Ref.
O1	20	15	1.8	0.5	590	390	3.0	[9]
O2	72	30	40	-23.5	397	410	3.0	[10]
O3	110	75	100	-46.9	190	410	2.9	[9]
O4	220	150	300	-46.7	59	320	3.6	[9]
O5	400	400	1000	-250	21	240	4.2	[11]
O6	500	500	1245	-321	28	271	4.3	[12]
O7	765	550	2718	-449	12	274	4.1	[12]
O8	1000	650	4149	-260	11	267	4.4	[13]
U1	0.4	0.2	0.2	0.15	127	82	220	(2)
U2	20	10	7	10.4	98	119	96	[14]
U3	72	50	50	31.3	21	191	110	[15]
U4	110	60	100	89.6	21	111	73	[16]
U5	220	40	400	373	19	157	72	[17]
U6	400	20	1200	2115	14	180	75	[18]
U7	500	20	2000	2934	11	203	64	[19]
G1	170	50	400	351	18	59	19	[12]
G2	300	100	1e3	440	16	66	16	[12]
G3	400	100	2e3	1039	6.3	64	17	[11]
G4	800	150	5e3	2359	10	78	14	[12]
G5	1200	150	1e4	6770	8	65	13	[12]

(1) O = overhead, U = underground/submarine, G = gas insulated.
(2) Prepared by the authors.

TABLE 2. Values of κ and τ for the lines of Table 1.

Name	κ	$\tau \times 10^4$	Name	κ	$\tau \times 10^4$
O1	1.51	4.33	U3	0.11	265
O2	0.97	10.7	U4	0.19	151
O3	0.46	40.6	U5	0.12	91.6
O4	0.18	134	U6	0.08	27.2
O5	0.09	801	U7	0.05	26.0
O6	0.10	1435	G1	0.31	15.3
O7	0.04	1652	G2	0.24	55.9
O8	0.04	2378	G3	0.10	54.9
U1	1.55	0.012	G4	0.13	124.6
U2	0.82	0.96	G5	0.12	96.3

A. LINE LOADABILITY

Regarding the behavior of lines in terms of active/reactive power flows, assuming that the sending voltage is equal to the rated voltage, it is customary to separately consider two idealized boundary constraints at the receiving bus, namely: 1) the voltage is specified (PV bus) and 2) the reactive power consumption is specified (PQ bus). In practice, the actual operating condition will lie somewhere between those extreme cases, depending on the type of line. For instance, a line belonging to a strongly meshed transmission system may be closer to the PV case, whereas a radial distribution line will be better characterized by the PQ-bus assumption. Both cases are considered below when analyzing the loadability from the steady-state stability viewpoint.

1) RECEIVING PV BUS

The maximum active power that can reach the receiving end for a given voltage (PV bus) can be obtained from (11) as

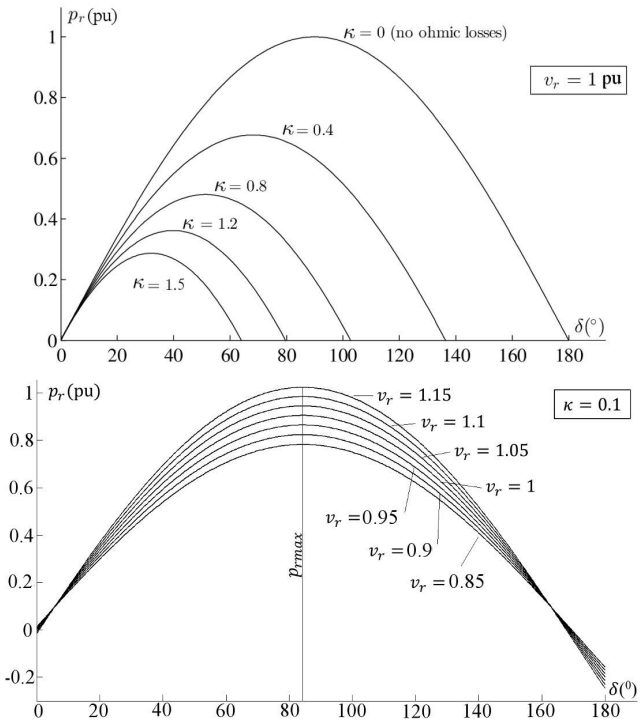

FIGURE 2. $p_r - \delta$ curves for different values of κ with $v_r = 1$ pu (top) and for different values of v_r with $\kappa = 0.1$ (bottom).

follows:

$$\partial p_r/\partial\delta = 0 \;\Rightarrow\; \delta_{max} = \arctan(1/\kappa)$$
$$p_{rmax} = v_r\sqrt{1+\kappa^2} - \kappa v_r^2 \,. \tag{22}$$

This limit depends to a greater extent on κ and to a lesser extent on v_r, as can be seen in Fig. 2, that shows the curves of $p_r(\delta)$ for different values of κ, with $v_r = 1$ pu (top), and for different values of v_r with $\kappa = 0.1$ (bottom).

In the lossless case ($\kappa = 0$), $p_{rmax} = v_r$. Therefore, if the receiving voltage is maintained at the rated voltage ($v_r = 1$), then the maximum active power that can reach the receiving bus is exactly the SSL ($p_{rmax} = 1$). But the same maximum power could be achieved in the lossy cases provided that $v_r > 1$. It is worth noting that for $v_r \leq 1$ all the curves $p_r - \delta$ have a common point at $\delta = \arccos v_r$, regardless of the value of κ. Needless to say, angles larger than δ_{max} correspond to infeasible steady-state operating points. In practice, a tighter limit than the SSL value is customarily imposed, in an attempt to address transient stability issues (e.g., sudden loss of a reactive power compensator near the receiving end). For instance, $\delta = \delta_{max}/2$ is assumed in Table 1 to determine the maximum active power of lines O6, O7 and O8 (δ_{max} is 84° for O6 and 88° for O7 and O8), but more conservative values, such as $\delta = \delta_{max}/3$, are frequently found in the literature.

2) RECEIVING PQ BUS

The $p_r(\delta)$ curves can also be obtained by imposing a given load power factor ($\cos\varphi$) at the receiving bus (PQ bus).

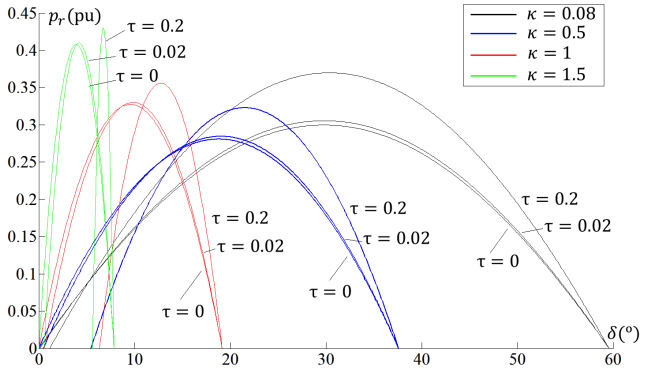

FIGURE 3. $p_r - \delta$ curves for different values of κ and τ with $\cos\varphi = 0.9$.

Eliminating v_r by combining (11)-(12):

$$v_r = \frac{(1-\kappa\tan\varphi)\cos\delta - (\kappa+\tan\varphi)\sin\delta}{1-\tau-\kappa\tan\varphi}\,, \tag{23}$$

leads to an expression of p_r, not shown due to its complexity, which is depicted in Figure 3 for representative values of κ and τ. In this case, the maximum transmitted active power is roughly half the maximum value obtained for the PV-bus case. Note that the parameter τ affects the curves only slightly, whereas the influence of κ is higher, much like in Figure 2 (top).

B. LINE EFFICIENCY

From (9) and (11) the universal line efficiency expression is given by

$$\eta = \frac{P_r}{P_s} = \frac{p_r}{p_s} = \frac{\sin\delta + \kappa(\cos\delta - v_r)}{\sin\delta - \kappa(\cos\delta - 1/v_r)}\,. \tag{24}$$

Figure 4 represents the efficiency versus κ for different values of δ and two values of v_r, namely $v_r = 1$ (solid line) and $v_r = 0.9$ (dashed line). As expected, the losses are null ($\eta = 1$) for $\kappa = 0$. For $\delta > 0$, it can be shown that, for any $v_r < 1$, the respective η curve intersects with that for $v_r = 1$ exactly when $\eta = v_r$. This can be observed in the figure, where the efficiency curves for $v_r = 1$ and $v_r = 0.9$ intersect, for a given $\delta > 0$, at $\eta = 0.9$.

C. REACTIVE POWER BALANCE

In this subsection, the line behavior regarding the generation/consumption of reactive power is analyzed for the PV and PQ receiving end cases.

1) RECEIVING PV BUS

In the PV-bus case, for a given v_r, the reactive power balance of the line depends on the values of τ and δ. For small values of τ and δ, the first term of (20) is comparable to the second one, resulting in a narrow range of reactive power consumption/generation. On the contrary, for larger values of τ and δ the first term of (20) is lower and the second term is higher, giving rise to a wider range of reactive power consumption/generation.

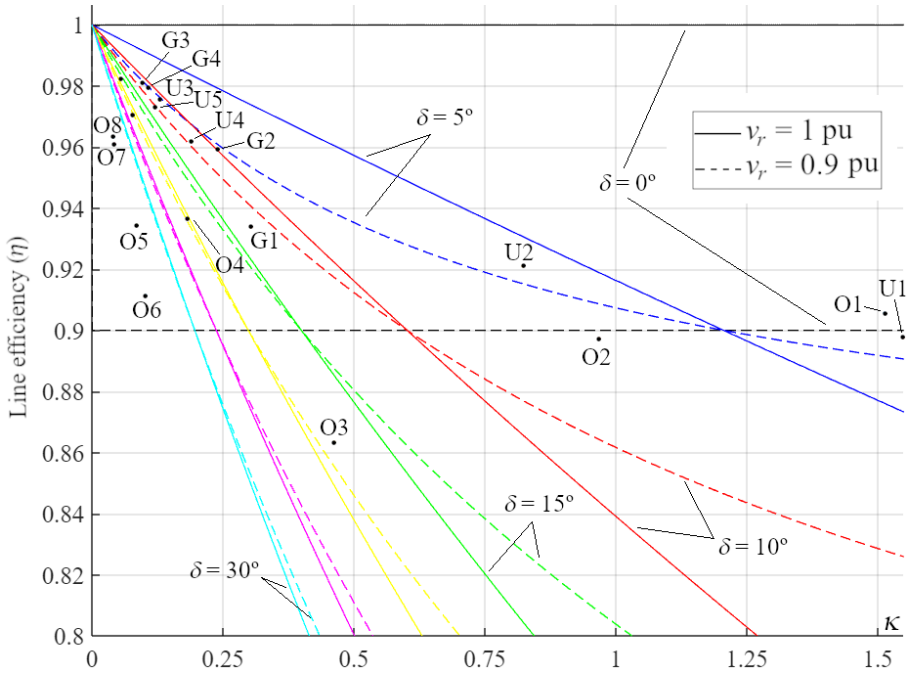

FIGURE 4. Line efficiency as a function of κ and δ for two values of v_r.

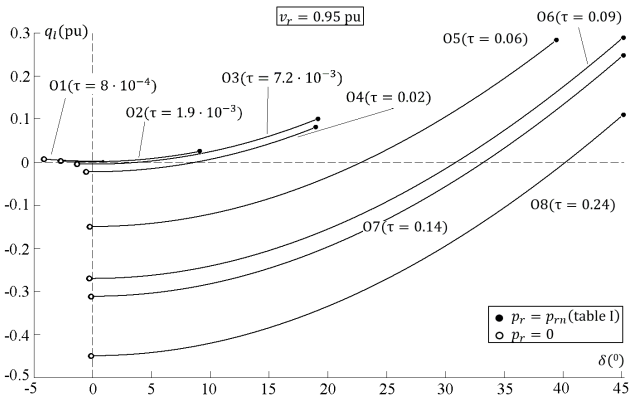

FIGURE 5. Curves $q_l - \delta$ for different values of τ through the whole load range of the overhead lines in Table 1 (v_r = 0.95 pu).

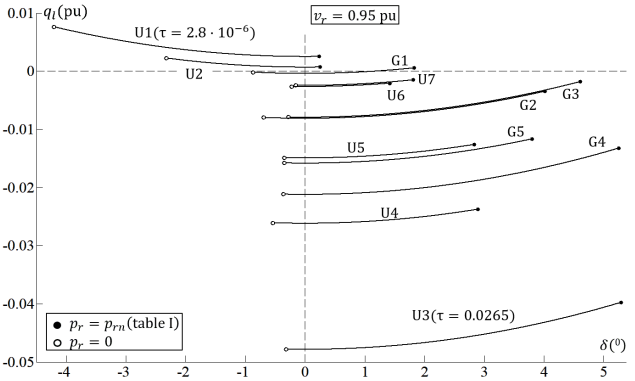

FIGURE 6. Curves $q_l - \delta$ for different values of τ through the whole load range of the underground/submarine and GIL lines in Table 1 (v_r = 0.95 pu).

This is better observed in Figures 5 (overhead lines) and 6 (rest of lines), where q_l is depicted versus δ for the values of τ corresponding to the whole set of lines in Table 1, when $v_r = 0.95$ pu (qualitatively similar results are obtained for $v_r \approx 1$).

In Figure 5, the medium voltage overhead lines (O1, O2) consume/generate a small amount of reactive power in the whole loading range (for $v_r \approx 1$) due to the small values of τ and δ. On the contrary, for high voltage overhead lines (O3 to O8) both terms of (20) may become quite different, leading to a much wider range of q_l values.

For the underground/submarine and GIL lines (Figure 6), typically shorter than overhead lines, the conclusion is similar to that of the medium voltage lines, O1 and O2. In these cases, τ is small (it ranges from $2.8 \cdot 10^{-6}$ to 0.0265), so the first term of (20) is large, but the values of δ are also low (second term of (20) non negligible), leading to relatively small reactive power imbalances. Accordingly, the range of variation between the loaded and unloaded cases is quite narrow, owing to the small range of variation of δ. As expected, as shown in Figure 6, the value of q_l is mostly negative (surplus of reactive power). Be aware that, owing to the normalization of magnitudes, the scales of q_l in figures 5 (overhead lines) and 6 (GIL and underground lines) are quite different, so directly comparing the q_l values from both figures can be misleading.

2) RECEIVING PQ BUS

In the PQ-bus case, v_r can be eliminated from (20), by means of (23). This way, q_l becomes a function of δ, the power factor at the receiving end and the parameters κ and τ. Assuming $\cos\varphi = 0.9$, the functions $q_l(\delta)$ are represented in Figure 7

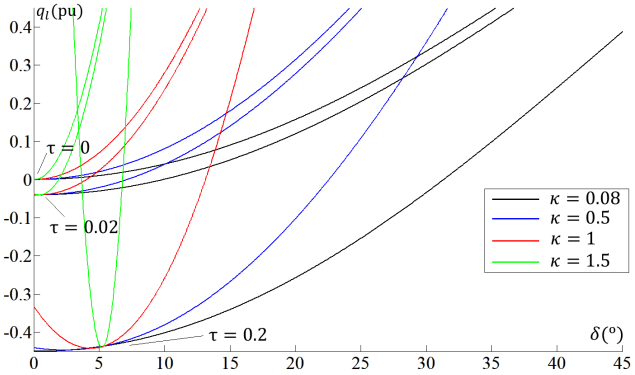

FIGURE 7. PQ bus: $q_l - \delta$ curves for $\cos\varphi = 0.9$ and different values of κ and τ.

for the same values of κ and τ as in Figure 2. In contrast to Figure 2, τ is more influential in this case than κ in relation to the overall reactive power of the line. For light loads, there is an excess of reactive power, which intensifies for increasing values of τ and alleviates for increasing line loadings.

D. ACTIVE POWER FLOW THAT BALANCES THE REACTIVE POWER REQUIREMENTS OF THE LINE

In Figures 5 and 6 the horizontal axis ($q_l = 0$) corresponds to the case in which the reactive power consumption of the series inductance is offset by the reactive power supplied by the shunt capacitance. Let p_{r0} denote the real power delivered by the line when $q_l = 0$. In the lossless case, this operating point is termed the "surge impedance loading" (SIL), which is a reference or representative point worth characterizing. Figure 8 represents p_{r0} against τ for different values of κ and $v_r = 0.95$ (similar results are obtained for $v_r \approx 1$). The cases O1, O2, U1 and U2 of Table 1 are not shown, since $q_l = 0$ leads to an infeasible case, with no real solution for p_{r0}.

The normalized loadability limits (p_{rn}), provided in Table 1, are also shown in Figure 8. For the overhead lines considered, p_{rn} is always higher than p_{r0}, which means that external reactive power support will be needed to deliver such levels of active power. Note, however, that for longer lengths than those assumed in Table 1 (higher values of τ) the loadability limit might become lower than p_{r0}, which is uneconomic.

On the other hand, for underground/submarine and GIL lines it is generally verified that $p_{rn} < p_{r0}$, meaning that a surplus of reactive power will always exist, regardless of the line loading. A notable exception is the line G1, that behaves much like an overhead line in this regard. This opens up the possibility of designing GIL lines at other voltages and lengths with a view to keeping the reactive unbalance at low levels.

It is possible to obtain an approximate yet accurate enough analytic expression for $p_{r0}(v_r)$ by equating (20) to zero, from which

$$\cos\delta_0 = \frac{1+v_r^2}{2v_r}(1-\tau) \approx 1-\tau \ , \tag{25}$$

$$\sin\delta_0 \approx \sqrt{\tau(2-\tau)} \ , \tag{26}$$

The above approximations are acceptable as long as v_r remains close to 1 (the practical case). For example, for $v_r = 0.95$ the error in the approximation is 0.1%. Replacing (25) and (26) into (11) yields

$$p_{r0}(v_r) \approx v_r\left(\sqrt{\tau(2-\tau)} + \kappa(1-\tau-v_r)\right) . \tag{27}$$

Note that, for the particular value $\tau = 1 - v_r$, the second term in (27) vanishes and p_{r0} is not a function of κ (as shown by the common point for all curves in Figure 8).

In the lossless case ($\kappa = 0$), p_{r0} reduces to the well-known SIL concept, for which the following simplified expression is obtained in terms of normalized parameters:

$$SIL \approx v_r\sqrt{\tau(2-\tau)} \approx v_r\sqrt{2\tau} \ . \tag{28}$$

E. CHARGING CURRENT

The charging current i_{sc} of a line is the current at the sending end with no load at the receiving end ($p_r = q_r = 0$). In some cases (typically in long cables) this unavoidable current can be so large that the remaining ampacity gets drastically reduced. By equating (11) and (12) to zero, the expressions for the no-load voltage at the receiving end and the real, reactive and apparent powers at the sending end are obtained. A further simplification is made by taking into account that $\tau \ll 2$, leading to:

$$p_{sc} \approx \frac{\kappa\tau^2}{1+\kappa^2-2\tau} > 0 \ , \tag{29}$$

$$q_{sc} \approx -\tau\frac{2+2\kappa^2-3\tau}{1+\kappa^2-2\tau} \ , \tag{30}$$

$$i_{sc} = s_{sc} \approx 2\tau\frac{\sqrt{1+\kappa^2-\tau}}{\sqrt{1+\kappa^2-2\tau}} \ , \tag{31}$$

where p_{sc} and q_{sc} denote the active and reactive power at the sending end when $p_r = q_r = 0$.

The maximum error of the above approximations for the heterogeneous set of lines included in Table 1 is less than 1.5 %, except for the UHV long line O8, which is 4 %.

Figure 9 shows the curves of i_{sc} versus τ for different values of κ. The i_{sc} values for the lines of Table 1 are shown as filled circles. In the same figure, the values of the current i_{smax}, corresponding to the maximum load p_{rn} for each line in Table 1, are also depicted as empty circles. The figure clearly shows a higher dependency of i_{sc} on τ than on κ (the curves are quite close to each other). In fact, all the points corresponding to the lines of Table 1 lie virtually on the curve for $\kappa = 0$. The figure is also interesting to ascertain at a glance the relative importance of the no-load current over the maximum current, by comparing each filled circle with the empty one located right above. For the cases of Table 1, some lines like U3 or O8 have a significant no-load current that must be assessed and ultimately compensated, as it is well known.

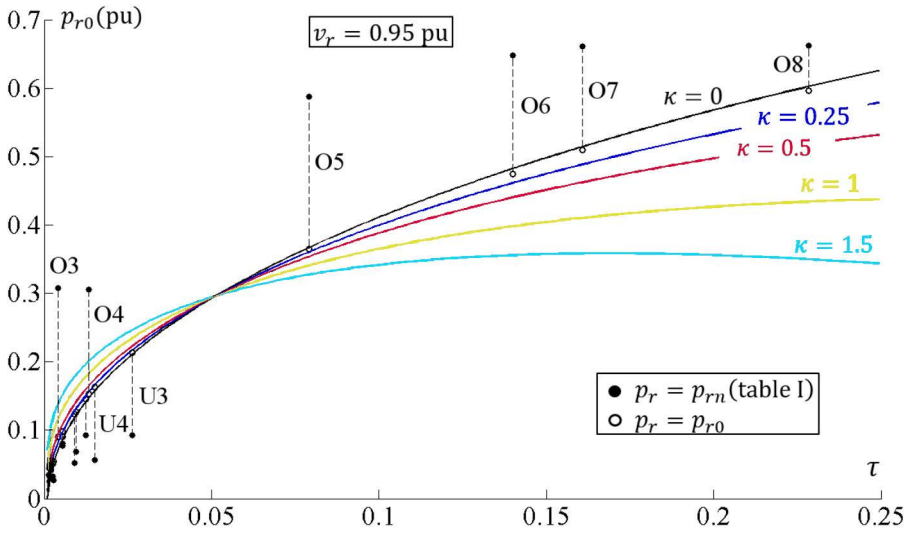

FIGURE 8. Curves p_{r0} versus τ for $v_r = 0.95$ pu and different values of κ, along with values of p_{r0} and p_{rn} for the cases of Table 1 (whenever p_{r0} exists).

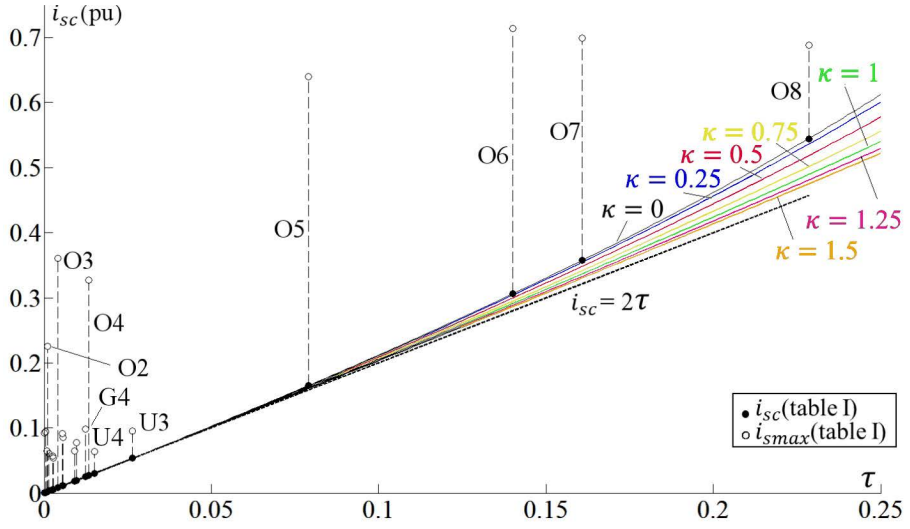

FIGURE 9. Curves of charging current i_{sc} versus τ for different values of κ.

For underground and GIL cases, the expression for i_{sc} can be further simplified by noting that $\tau \approx 0$:

$$i_{sc} \approx 2\tau \frac{\sqrt{1+\kappa^2-\tau}}{\sqrt{1+\kappa^2-2\tau}} \approx 2\tau \ , \tag{32}$$

The validity of this approximation can be checked in Figure 9, where the linear function $i_{sc} = 2\tau$ is also represented.

F. FERRANTI EFFECT

Under the same no-load conditions of the previous section ($p_r = q_r = 0$), taking into account that $\tau \ll 2$, the voltage at the receiving end can be obtained from

$$v_{rc} = \frac{\sqrt{1+\kappa^2}}{\sqrt{1+\kappa^2-2\tau+\tau^2}} > 1, \tag{33}$$

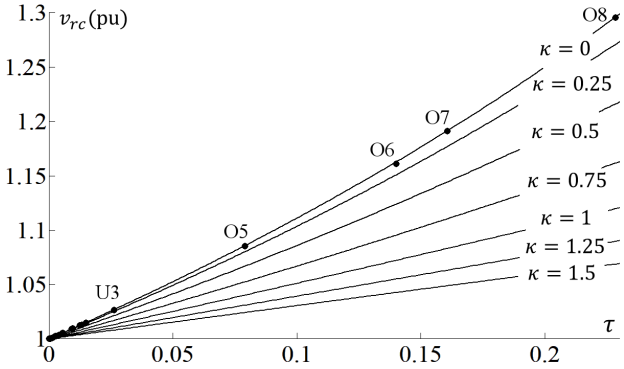

FIGURE 10. Voltage at the open receiving end for different values of κ. The circles correspond to the values of Table 1.

which reflects the well-known Ferranti effect (open-circuit receiving end voltage always higher than the sending end

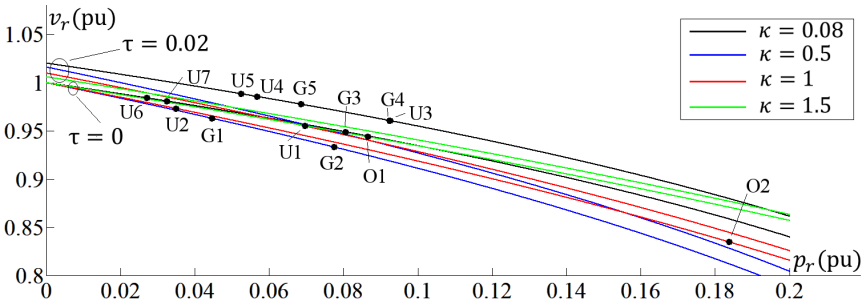

FIGURE 11. PV generic curves for $\cos\varphi = 0.9$ and some points of Table 1.

voltage), more noticeable for lines with higher values of τ (long overhead lines). The receiving end voltage is represented in Figure 10 as a function of τ for different values of κ. The voltages corresponding to the lines of Table 1 are also shown as circles.

G. PV AND QV CURVES

By resorting only to κ and τ it is possible to obtain nearly exact generalized PV (nose) curves, where the receiving (unregulated) bus voltage is represented versus p_r for a given load power factor ($\cos\varphi$). Eliminating δ from (11) and (12) yields,

$$v_r^2 = \frac{1}{2F}\left(E \pm \sqrt{F^2 - 4p_r^2(1+\tan^2\varphi)F}\right), \quad (34)$$
$$E = 1 + \kappa^2 - 2p_r\left[\kappa + (1-\tau)\tan\varphi\right],$$
$$F = \kappa^2 + (1-\tau)^2.$$

Figure 11 shows the PV curves (upper part of the nose) for representative values of κ and two values of τ: 0 (representative of O1, O2, U1, U2, U6, U7, G1, G2, G3) and 0.02 (U3, U4, U5, G4, G5), assuming an inductive power factor $\cos\varphi = 0.9$ (the typical case of a radial line with non regulated voltage at the load end). Moreover, the figure shows the points of maximum active power P_{rn} of Table 1 and $\cos\varphi = 0.9$. For the lines O3-O8, the P_{rn} values shown in Table 1 are infeasible for a load with $\cos\varphi = 0.9$ inductive (in fact, the reactive power at the receiving end should be negative, i.e. injected, for the operating points in the Table to be feasible). The PV curves corresponding to those lines are separately shown in Figure 12, where the infeasible points of active power P_{rn} and $\cos\varphi = 0.9$ are also represented.

From (34), it can be easily verified that $v_r = 1$ for $p_r = 0$ and $\tau = 0$, regardless of the value of κ.

The QV curves can also be obtained for different values of κ and τ. These curves represent the required reactive power to be injected ($q_r < 0$) or drawn ($q_r > 0$) at the receiving end versus v_r for a given p_r value. The required relationship can be obtained by eliminating δ from (11) and (12), yielding:

$$q_r = \tau + \sqrt{v_r^2(1+\kappa^2(1-v_r^2)) - p_r^2 - 2\kappa p_r v_r^2} - 1 \quad (35)$$

As an example, Figure 13 shows the QV curves for $p_r = 0$. From (35) it is immediately concluded that $q_r = \tau$ for

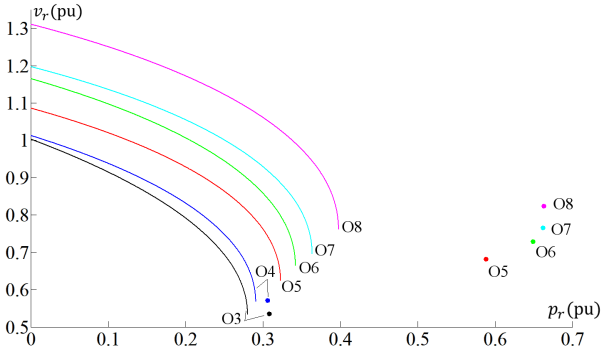

FIGURE 12. PV curves with $\cos\varphi = 0.9$ for the lines O3-O8 of Table 1 and their corresponding points.

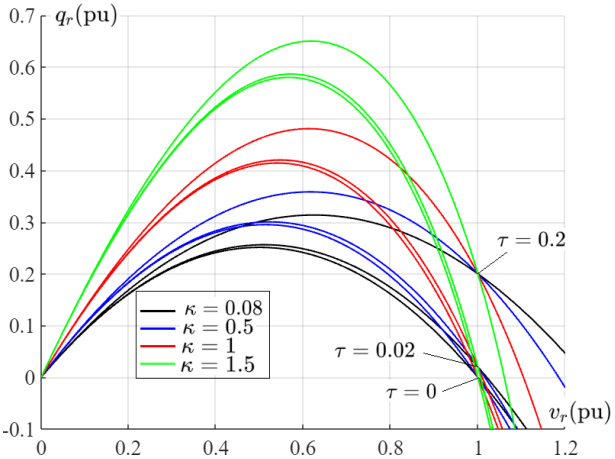

FIGURE 13. QV generic curves for $p_r = 0$. The curves with common τ are crossing the point (1, τ).

$p_r = 0$ and $v_r = 1$, which is confirmed in the figure. This provides another interpretation for τ: the amount of (normalized) reactive power that must be drawn from the line at the receiving end to avoid the Ferranti effect at no load.

H. PQ CURVES

Other typical curves related to lines are those representing q_r versus p_r for a given value of v_r, for which (35) is still of application when v_r is replaced by a constant value. For example, for $v_r = 1$, (35) reduces to,

$$q_r = \sqrt{1 - 2\kappa p_r - p_r^2} + \tau - 1. \quad (36)$$

VI. CONCLUSION

This paper has reconsidered the distributed-parameter, steady-state model of AC power lines in an attempt to develop a unified yet simple parameterized framework, from which the behavior of any power line, regardless of its type (overhead, underground, GIL), rated voltage and length, can be algebraically and graphically characterized. It is shown that only two dimensionless parameters (κ and τ) are involved in the proposed generalized model (assuming the shunt conductance is negligible). Normalized power flows at both line terminals are inferred, allowing universal parameterized curves to be obtained for any electrical magnitude of interest, such as line losses, efficiency, no-load receiving end voltage and charging current, surge impedance loading, steady-state stability limit or PV, QV and PQ curves. The use of those parameters, which remain bounded in a known interval for all lines of practical interest, provides a more comprehensive and integrated understanding of the major issues at stake, when compared with the customary approach that segments lines by type, rated voltage and length. In addition to educational or academic uses, the universal model proposed in this work can be useful for planners and operators. For planners because, once they determine that the transmission capacity of a given congested corridor should be expanded, the dimensionless model can help them select the optimal arrangement among the several feasible choices. For operators because, given a power flow solution, or the state provided by an estimator in the EMS, they could perform an accurate ex-post graphical analysis of the performance (losses, closeness to the collapse point, etc.) of the different lines in the network, regardless of their type.

REFERENCES

[1] T. Gönen, *Electric Power Transmission System Engineering: Analysis and Design*, 2nd ed. Boca Raton, FL, USA: CRC Press, 2009.

[2] H. P. S. Clair, "Practical concepts in capability and performance of transmission lines [includes discussion]," *Trans. Amer. Inst. Electr. Eng. III, Power App. Syst.*, vol. 72, no. 6, pp. 1152–1157, Dec. 1953, doi: 10.1109/AIEEPAS.1953.4498751.

[3] R. D. Dunlop, R. Gutman, and P. P. Marchenko, "Analytical development of loadability characteristics for EHV and UHV transmission lines," *IEEE Trans. Power App. Syst.*, vol. PAS-98, no. 2, pp. 606–617, Apr. 1979, doi: 10.1109/TPAS.1979.319410.

[4] D. Lauria and S. Quaia, "Loadability of 400 kV four-bundled overhead transmission lines," presented at the Int. Conf. Clean Electr. Power (ICCEP), Taormina, Italy, Jun. 2015.

[5] D. Lauria, F. Mottola, and S. Quaia, "Analytical description of overhead transmission lines loadability," *Energies*, vol. 12, pp. 1–18, Jan. 2019, doi: 10.3390/en12163119.

[6] C. S. Schifreen and W. C. Marble, "Charging current limitations in operation or high-voltage cable lines [includes discussion]," *Trans. Amer. Inst. Electr. Eng. III, Power App. Syst.*, vol. 75, no. 3, pp. 803–817, Jan. 1956, doi: 10.1109/AIEEPAS.1956.4499370.

[7] G. E. Balog, G. Evenset, and F. Rudolfsen, "Energy transmission on long three core/three foil XLPE power cables," in *Proc. Jicable*, Versaille, France, 2003, pp. 256–261.

[8] J. Song-Manguelle, M. H. Todorovic, S. Chi, S. K. Gunturi, and R. Datta, "Power transfer capability of HVAC cables for subsea transmission and distribution systems," *IEEE Trans. Ind. Appl.*, vol. 50, no. 4, pp. 2382–2391, Jul. 2014, doi: 10.1109/TIA.2013.2291934.

[9] *Power Engineering Guide, Version 7.1*, Siemens, Erlangen, Germany, 2014.

[10] J. Hao and W. Xu, "Extended transmission line loadability curve by including voltage stability constraints," presented at the Electr. Power Energy Conf., Vancouver, BC, Canada, Oct. 2008.

[11] D. Lauria and S. Quaia, "Technical comparison between a gas-insulated line and a traditional three-bundled OHL for a 400 kV, 200 km connection," presented at the Int. Conf. Clean Electr. Power, Taormina, Italy, Jun. 2015.

[12] D. Khan, M. Rafiq, S. Furqan, I. Khan, and F. Abbas, "Comparison of tranmission losses and voltage drops of GIL (gas insulated transmission line) and overhead transmission lines," in *Proc. Int. Power Electron. Motion Control Conf. Expo.*, Antalya, Turkey, Sep. 2014, pp. 1–3.

[13] H. Huang, D. Kumar, V. Ramaswami, and D. Retzmann, "UHV 1200 kV AC transmission," presented at the GridTech, New Delhi, India, Feb. 2007.

[14] *6-36kV Medium Voltage Underground Power Cables*, Nexans, Paris, France, 2010.

[15] *XLPE Land Cable Systems. User's Guide Version 5*, ABB, Zürich, Switzerland, 2010.

[16] M. Zubiaga, G. Abad, J. A. Barrena, S. Aurtenetxea, and A. Cárcar, *Energy Transmission and Grid Integration of AC Offshore Wind Farms*, Rijeka, Croatia: Intech Open, 2012.

[17] K. Barber, "Achievement and experience in service of long length high voltage AC electrical links by insulated power cables," presented at the Latin Amer. Workshop Insulated Cables, Foz do Iguaçu, Brasil, Sep. 2013.

[18] F. M. Gatta and S. Lauria, "Very long EHV cables and mixed overhead-cable lines. steady-state operation," in *Proc. IEEE Russia Power Tech*, St. Petersburg, Russia, Jun. 2005, pp. 1–7.

[19] M. del Brennna, F. Donazzi, and A. Mansoldo, "Long length EHV underground cable systems in the transmission network," in *Proc. Session Cigré*, Paris, France, Aug. 2004, pp. 1–9.

PEDRO CRUZ-ROMERO (Member, IEEE) received the Ph.D. degree in electrical engineering from the University of Seville, Spain, in 2000. Currently, he is an Associate Professor at the University of Seville. His research interests include transmission and distribution analysis and design. He has been a member of Cigré, since 2002.

ANTONIO GÓMEZ-EXPÓSITO (Fellow, IEEE) received the Electrical Engineering and Ph.D. degrees (Hons.) from the University of Seville, in 1982 and 1985, respectively. Since 2007, he has been the Endesa Red Chair Professor at the University of Seville. In addition to some 350 technical publications, he has coauthored a dozen textbooks and monographs about circuit theory and power systems, among which *Power System State Estimation: Theory and Implementation* (New York: Marcel Dekker, 2004) and *Electric Energy Systems: Analysis and Operation* (Boca Raton, FL, USA: CRC Press, 2008, 2nd edition 2018), stand out. In 2019, he received the IEEE/PES Outstanding Power Engineering Educator Award. He served on the Editorial Board of the IEEE TRANSACTIONS ON POWER SYSTEMS, from 2011 to 2016. He is currently the Vice Editor-in-Chief of the *Journal of Modern Power Systems and Clean Energy*.

JUAN CARLOS DEL-PINO-LÓPEZ received the Ph.D. degree in electrical engineering from the University of Seville, Spain, in 2010. Currently, he is an Associate Professor at the University of Seville. His research interest includes the application of finite element analysis to multiphysics problems in power systems.